

Pyrrhotite-related $\text{Fe}_x(\text{Se}_{1-y}\text{Te}_y)_8$; $x \approx 7$, $y \leq 0.15$ solid solutions, studied by X-ray diffraction, magnetization and Mössbauer spectroscopy techniques

TORE ERICSSON¹, ÖRJAN AMCOFF¹ and PER NORDBLAD²

¹University of Uppsala, Institute of Earth Sciences, Mineralogy-Petrology, Norbyvägen 18 B, S-752 36 Uppsala, Sweden

²University of Uppsala, Department of Technology, Box 534, S-751 21 Uppsala, Sweden

Abstract—Pyrrhotite-related $\sim\text{FeX}$; X = Se, Te, S compounds with compositions in the range of Fe_7Se_8 have been synthesized. At 873 K the solubility of Te in Fe_7Se_8 is between 15 and 20 mole%, decreasing to less than one mole% at 423 K. The corresponding solubility of Te in hexagonal Fe_7S_8 is less than one mole% at 873 K. Vacancy ordering in Fe_7Se_8 (*1c*), giving rise to a hexagonal *3c*-superstructure in rapidly cooled samples, is more strongly hindered by Te-substitution compared with S-substitution; however, Mössbauer spectroscopy indicates local ordering of vacancies. These phenomena can be seen as a change in the macroscopic magnetization. They can be modelled by a continuous decrease in the size of the vacancy-ordered domains with Te-substitution (and to a lesser degree with S-substitution), as a result of domain-walls being arrested by the foreign atoms. Also, a characteristic spin re-orientation takes place at 130 K in Fe_7Se_8 (*3c*), with spins turning from the *ab* plane to the *c*-axis on lowering the temperature. The temperature for this re-orientation is increased when Se is substituted by Te (and decreased when Se is substituted by S), reflecting the corresponding change in relative magnitude of the distances between neighbouring Fe-atoms.

INTRODUCTION

IRON SULFIDES are quantitatively the most important sulfide minerals in nature. In mineralizations formed in near surface environments both pyrite and pyrrhotite are common, while the latter phase dominates in mafic and ultramafic igneous rocks because of a low oxygen fugacity. As a consequence, pyrrhotite can be expected to be of widespread occurrence in the mantle.

Pyrrhotite-related compounds show a considerable complexity, especially at low and intermediate temperatures, as seen both in nature and in the synthetic Fe-S system; thus, the mineral has been much studied (*e.g.*, THIEL, 1969, VAUGHAN and CRAIG, 1978, KISSIN and SCOTT, 1982, BARKER and PARKS, 1986 and KULLERUD, 1986).

Studies of compositions along the pseudobinary $\text{Fe}_7\text{S}_8 - \text{Fe}_7\text{Se}_8$ join (ERICSSON *et al.*, 1994) show that the low field magnetic permeability decreases gradually inwards from both end compositions. This indicates a change from ordered to disordered structure with an increase in (S,Se)-mixing, a finding that was supported by X-ray diffraction (XRD). However, Mössbauer spectroscopy (MS) indicated local ordering throughout the solid solution series. We explain these superficially contradictory results by assuming a model where the size of the ordered regions in the mix crystals decreases continuously as the middle composition along the $\text{Fe}_7\text{S}_8 - \text{Fe}_7\text{Se}_8$ join is approached. This yields a corresponding decrease in the low field permeabil-

ity inwards if it is assumed that the ferromagnetic coupling within an *ab* layer is intact over the phase - antiphase boundaries.

In the present paper we have pursued our studies on pyrrhotite-like compounds further and investigated the effect of anion-mixing by introducing Te into the system. Of special interest is the question of how a spin re-orientation, from the *ab*-plane to the *c*-axis with decreasing temperature, is affected by Te/Se-substitution. This substitution is assumed to be completely random, as in the case of compositions along the $\text{Fe}_7\text{S}_8 - \text{Fe}_7\text{Se}_8$ join (ERICSSON *et al.*, 1994).

CRYSTAL STRUCTURE AND MAGNETIC PROPERTIES

In the hexagonal structure, which is NiAs-related, the iron deficiency is compensated by vacancies, which at elevated temperatures are statistically distributed among the cations giving a primitive *1c*-structure. Because of vacancy avoidance (BERTAUT, 1953) superstructures form on lowering the temperature, and the lattice multiplicity of the supercell depends both on composition and temperature (PUTNIS and MCCONELL, 1980).

Compositions near Fe_7S_8 yield superstructures where the *a*-axis is repeated twice and the *c*-axis three or four times (*3c* or *4c*), depending on heat treatment. In the analogous Fe-Se system a similar situation is present for compositions around Fe_7Se_8 . In the primitive *1c*-structure, the magnetic

moments are ferromagnetically coupled (FM) within a cation *ab*-layer, but antiferromagnetically coupled (AFM) between adjacent *ab*-layers, giving zero net moment for the crystal. On the other hand, the superstructures *3c* and *4c* show a ferrimagnetic moment (FiM), as the vacancies are concentrated in alternating *ab*-layers.

In the hexagonal unit-cell of Fe_7Se_8 composition, an Fe atom is surrounded by six Se atoms in octahedral configuration at 2.55 Å, and by two Fe atoms in the *c*-direction at 2.94 Å. In the same *ab*-plane as the studied Fe atom, there are six Fe atoms at 3.61 Å, and in the fourth shell there are 12 Fe atoms at 4.65 Å (AMCOFF *et al.*, 1994). The situation is described in Fig. 1. In the *3c* and *4c* superstruc-

tures, where the vacancies are concentrated in every second metal *ab*-layer, the nearest surrounding to an Fe-atom can be described as being of A-, B- or C-type, as shown in the bottom part of Fig. 1. In the figure the numbers denote vacancies as well as heights in the *c*-direction (in *1c* units). The anion-layers have been excluded for clarity.

EXPERIMENTAL

Sample preparation and XRD

All preparations were undertaken using elements of 99.999% purity and employing the technique of dry synthesis in evacuated silica glass capsules. After weighing, loading and prereacting at 770 K for three days, each sample (0.5–1g) was ground under acetone and homogenized at 1073 K for one day. Subsequently one series was annealed at 873 K for one day and quenched, while a second series was annealed at 423 K for ten days and quenched.

Compositions yielding one-phase products after quenching in cold water from 873 K were: $y = 0.01, 0.05, 0.1$ and 0.15 , and $x = 7.08, 7$, and 6.92 in $\text{Fe}_x(\text{Se}_{1-y} \times \text{Te}_y)_8$. Prior to SQUID and MS measurements all samples were analysed using XRD with CuK_α radiation and Si as an internal standard ($a = 5.43088$ Å). Standard deviations of the obtained lattice parameters were less than 0.001 Å. Including a possible weighing error of 0.0005 g for each element, the errors in *c*- and *a*-axis data were calculated to be less than 0.004 Å and 0.002 Å, respectively. To avoid oxidation, all samples were stored under acetone between measurements.

SQUID

The magnetization measurements were performed in a Quantum Design MPMS5 SQUID magnetometer. The magnetization of each sample was measured in an applied field of 1 kOe versus temperature (10 – 300 K) and magnetization versus magnetic field curves were recorded at some different temperatures in fields 0–50 kOe.

Mössbauer spectroscopy

Transmission ^{57}Fe Mössbauer spectra (MS) were recorded at room and low temperatures, using a computerized spectrometer in constant acceleration mode. The establishment of the velocity scale was done using natural iron at room temperature as reference. The centroid shift CS is thus given relative to metallic Fe at 295 K. The source at room temperature was of CoRh-type. The powder absorbers contained less than 5 mg/cm² of natural Fe; thus we saw no need for thickness corrections when fitting the spectra using a locally developed Mössbauer fitting program (JERNBERG and SUNDQVIST, 1983). An Oxford Cryogenic helium flow cryostat, with a temperature stability better than ± 1 K, was used when measuring at low temperature.

ANALYSES AND RESULTS

Phase relations and lattice parameters

A NiAs-type iron selenide exists at low temperature with a composition around Fe_7Se_8

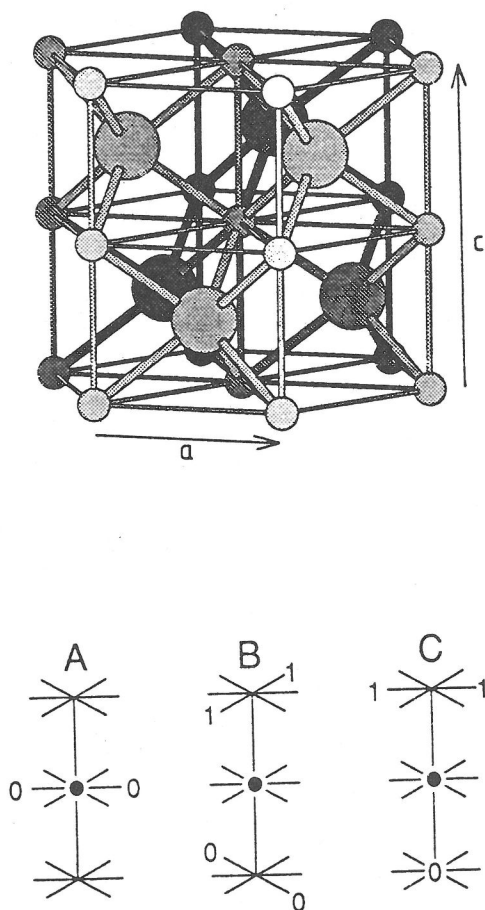


FIG. 1. Crystal structure of "NiAs,*1c*" and A, B, C vacancy configurations. In the upper figure (drawn by use of the program "ATOMS" by Shape Software), three primitive unit cells are shown. In the lower figure only the cation layers are sketched. The Mössbauer atom is black, and the numbers denote vacancies as well as heights in *c*-axis direction (primitive *1c*-units).

(SCHUSTER *et al.*, 1979; AMCOFF *et al.*, 1994), which shows complete solubility with pyrrhotite of Fe_7S_8 composition (ERICSSON *et al.*, 1994). On the other hand, NiAs-type phases in the Fe-Te system have Fe:Te ratios below 7:8, and are only stable above ~ 800 K (IPSER *et al.*, 1974). From this it can be deduced that the solubility of Te in Fe_7Se_8 must be limited.

Indeed, our results show a maximum solubility of between 15 and 20 mole% Te in $\text{Fe}_x(\text{Se}_{1-y}\text{Te}_y)_8$ for samples quenched from 873 K. Samples richer in Te decompose into a two-phase assemblage, with a Fe-rich PbO-type phase (composition around $\text{Fe}_{1.04}(\text{Se}_{1-y}\text{Te}_y)$) (AMCOFF *et al.*, 1994), plus a vacancy-rich phase, probably equivalent to a second NiAs-type phase which is distorted and present on the Se rich side of Fe_7Se_8 in the Fe-Se system (SCHUSTER *et al.*, 1979). Furthermore, employing an identical experimental procedure along an imaginary Fe_7S_8 - Fe_7Te_8 join, our results show a solubility of less than one mole% Te in pyrrhotite of Fe_7S_8 composition.

For pure Fe_7Se_8 , quenching in cold water from a high temperature (*e.g.*, 873 K) results in the formation of a well-ordered hexagonal superstructure (3c); while vacancy ordering is confined to smaller and smaller regions when S is substituted into the Se substructure. Slow cooling of the pure end-member phase, or annealing at *e.g.* 423 K, leads to formation of a triclinically distorted superstructure (4c). This transition fails in S-doped samples. Samples of $\text{Fe}_x(\text{Se}_{1-y}\text{Te}_y)_8$ compositions annealed at 423 K, with $x = 6.92, 7, 7.08$ and $y = 0.01, 0.05, 0.1, 0.15$, decomposed into the two-phase assemblage described above, except for one sample of composition $\text{Fe}_{6.92}(\text{Se}_{0.99}\text{Te}_{0.01})_8$. For this reason the discussion below is limited to "873 K samples."

When x is decreased at constant y in $\text{Fe}_x(\text{Se}_{1-y}\text{Te}_y)_8$, the c -axis in the basic unit cell contracts considerably more than the a -axis (Fig. 2). This finding is comparable with observed changes in pyrrhotites (KRUSE, 1990) and in Fe_xSe_8 (AMCOFF *et al.*, 1994). When y is increased at constant x in $\text{Fe}_x(\text{Se}_{1-y}\text{Te}_y)_8$ the a -axis expands in a regular way with increasing Te, while there is a smaller change in the c -axis. For the most vacancy-rich samples, $\text{Fe}_{6.92}(\text{Se}_{1-y}\text{Te}_y)_8$, the c -axis even contracts with increase in Te; possibly there is also such a tendency for Te-rich samples with $x = 7$ and 7.08 (Fig. 2).

Comparing the observed changes in lattice parameters with results from the pseudobinary Fe_7S_8 - Fe_7Se_8 join (ERICSSON *et al.*, 1994), it is obvious that the change in a -axis when Te is substituted into the Se-sublattice is more pronounced than with S-Te substitution (Fig. 3). This is not unexpected, since Se and

Te differ more, with regard to both ionic radius and electronegativity, than do Se and S. However, the decrease in the c -axis when Te is substituted for Se is unexpected. The rapid flattening of the unit cell (increase in a/c ratio) with increasing Te is probably related to the approach of the decomposition point, where the hexagonal phase is split into a PbO phase + a distorted NiAs phase.

Using XRD, $3c$ of Fe_7Se_8 composition can be distinguished from $1c$ by a set of well-defined superreflections (AMCOFF *et al.*, 1994). Two observations deserve to be mentioned in this connection: (i) With increasing Te, the superreflections decrease in intensity and disappear somewhere between $y = 0.05$ and $y = 0.1$ in $\text{Fe}_x(\text{Se}_{1-y}\text{Te}_y)_8$. We have

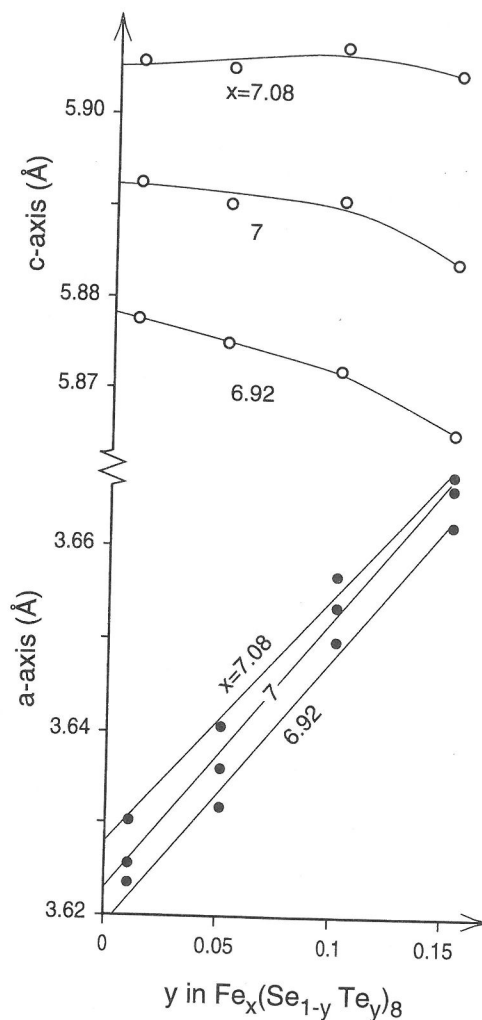


FIG. 2. Lattice parameter changes in $\text{Fe}_x(\text{Se}_{1-y}\text{Te}_y)_8$ mix crystals. The curves have been drawn by free-hand.

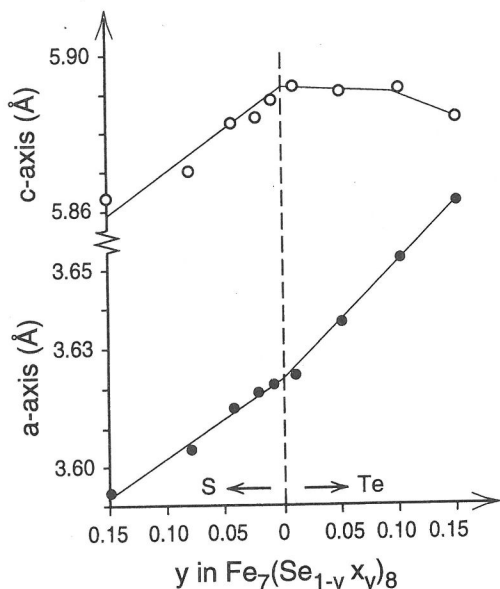


FIG. 3. Lattice parameter changes in $\text{Fe}_7(\text{Se},\text{X})_8$ around the pure end-composition, where X corresponds to S (to the left) and Te (to the right), respectively. Data for S/Se substitution have been taken from ERICSSON *et al.* (1994).

also noticed this phenomenon for compositions along the pseudobinary $\text{Fe}_7\text{S}_8\text{-Fe}_7\text{Se}_8$ join; but it is more accentuated for Se-Te substitution. (ii) With decreasing x (from 7), in $\text{Fe}_x(\text{Se}_{1-y}\text{Te}_y)_8$, the $3c$ -super-reflections become stronger, a finding which was also observed for compositions along the Fe-Se join (AMCOFF *et al.*, 1994). This can be explained partly by kinetics and partly by the fact that ideal $3c$ can only form in vacancy-rich samples (Fe_7X_8 according to *e.g.* (BERTAUT, 1953)).

Below, the lattice parameter changes as well as the changes in $3c$ -superreflection intensities are put in relation to the results from the magnetisation- and Mössbauer measurements.

SQUID

The magnetic response of $\text{Fe}_7(\text{Se}_{1-x}\text{Te}_x)_8$ is governed by the ferrimagnetic character of the sequential vacancy occupation in adjacent ab -planes. As in the case of substituting S for Se (ERICSSON *et al.*, 1994), the substitution of Te for Se hinders the occurrence of long range vacancy ordering, a vacancy ordering that characterises both the $3c$ and the $4c$ structures. However, a local ferrimagnetic order is evident on short length scales. The local magnetic structure remains essentially unchanged with Te substitution, whereas the macroscopic

magnetic response changes drastically, *e.g.*, the permeability decreases rapidly. Additionally, the temperature for the spin reorientation T_{sr} increases with increasing Te substitution. At T_{sr} , the spins flip from aligning parallel to the c -axis at low temperatures to being confined to the ab -plane at higher temperatures. We illustrate the macroscopic magnetic behavior by examining two details of the magnetic response that are highly sensitive to small compositional changes: (i) the temperature for the spin reorientation (occurring at $T \approx 130$ K for the pure selenium compound) and (ii) the low field permeability.

In Fig. 4, the magnetization at an applied field of 1 kOe is plotted versus temperature for some different samples. The magnetization is recorded after cooling the sample in zero field, applying the field at 10 K and then recording the magnetization with increasing temperature (zero field cooled procedure). The most striking feature of the curves is a marked increase of the magnetization with increasing temperature and an abrupt levelling off above a well defined temperature. We identify this knee in the curves as the spin reorientation temperature. It is seen from Fig. 4 that the magnetization (and consequently also the permeability) decreases rapidly with increasing Te substitution. In Fig. 5 we illustrate the permeability behaviour for the different samples by magnetization curves measured at 200 K. The macroscopic response changes from typical ferrimagnetic behaviour for the low Te contents to a linear response at higher Te content. This behaviour reflects the hindered vacancy ordering on increasing anion substitution.

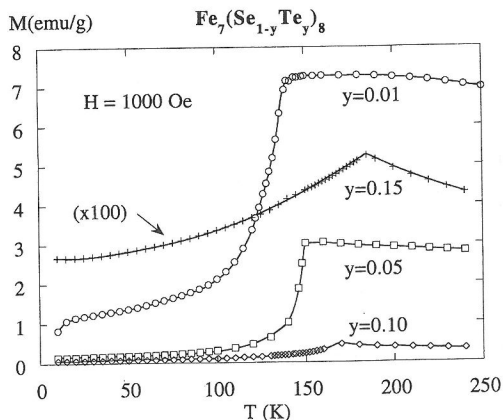


FIG. 4. Magnetization versus temperature at an applied field of 1 kOe for $\text{Fe}_7(\text{Se}_{1-y}\text{Te}_y)_8$ samples of different Te concentration. Note that the magnetisation for $y = 0.15$ has been multiplied by a factor of 100.

Fig. 6 shows M versus T and Fig. 7 M versus H curves for the nonstoichiometric compositions $\text{Fe}_{7.08}(\text{Se}_{0.95}\text{Te}_{0.05})_8$ and $\text{Fe}_{6.92}(\text{Se}_{0.95}\text{Te}_{0.05})_8$, together with the corresponding stoichiometric sample $\text{Fe}_7(\text{Se}_{0.95}\text{Te}_{0.05})_8$. As is seen from Fig. 6, the spin reorientation temperature decreases with an increasing number of vacancies and from Fig. 7 it is clearly seen that the saturation magnetisation increases with an increasing number of vacancies. The estimated saturation magnetisation scales reasonably well with the number of vacancies. At temperatures below T_{sr} , the material becomes magnetically softer with an increasing number of vacancies.

Mössbauer spectroscopy

Room temperature spectra. Spectra of Fe_7S_8 and Fe_7Se_8 recorded at room temperature are very similar in shape (ERICSSON *et al.*, 1994). LEVINSON and TREVES, (1968) presented a model for Fe_7S_8 in which the hyperfine field depends mainly on the number of Fe—S—Fe super-exchange bonds between iron in adjacent ab -planes. Fe atoms at A, B and C sites (see Fig. 1) have 18, 14, and 13 bonds (note that two near by Fe atoms along the same c -axis are connected via three Fe—S—Fe bonds), thus the hyperfine field for Fe at an A site should be larger than at a B site and smallest at a C site. The ferromagnetic coupling between the Fe atoms within the same ab -plane leads to a further division into A_1 (moment directed against a vacancy) and A_2 sites (moment directed against an Fe atom). The occurrence of the different configurations in the structure is $A_1:A_2:B:C = 1:2:2:2$.

We have used the four sextet model to fit all

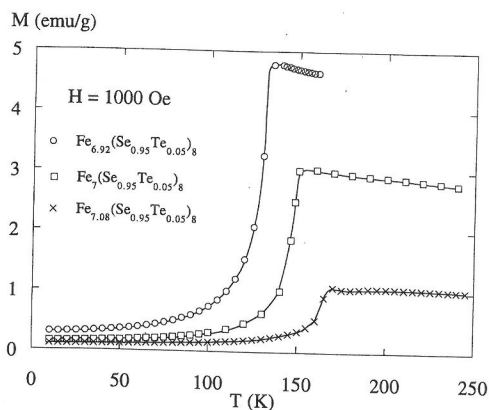


FIG. 6. Magnetization versus temperature at an applied field of 1 kOe for $\text{Fe}_x(\text{Se}_{0.95}\text{Te}_{0.05})_8$, three samples with $x = 6.92, 7$ and 7.08 .

spectra recorded at room temperature. It fits nicely for Fe_7Se_8 (AMCOFF *et al.*, 1994) and $\text{Fe}_7(\text{Se}_{0.99}\text{Te}_{0.01})_8$, and can still be used for Te-richer samples (Fig. 8). IGAKI *et al.* (1981; 1982) studied Fe_{1-x}S ($0.083 \leq x \leq 0.125$) by MS at room temperature and found that a vacancy in the same ab -plane increased the hyperfine field by 0.75 T (ΔB_a), a vacancy obliquely above (or below) decreased it by 0.875 T (ΔB_b) and a vacancy straight above (or below) along the same c -axis decreased it by 4.75 T (ΔB_c). The actual hyperfine field for a special configuration could then be calculated using a linear combination of ΔB_a , ΔB_b and ΔB_c , depending on the number of near-by vacancies. Transforming these values to Fe_7Se_8 leads to a reduction of $\approx 21\%$, thus $\Delta B_a = +0.59$ T, ΔB_b

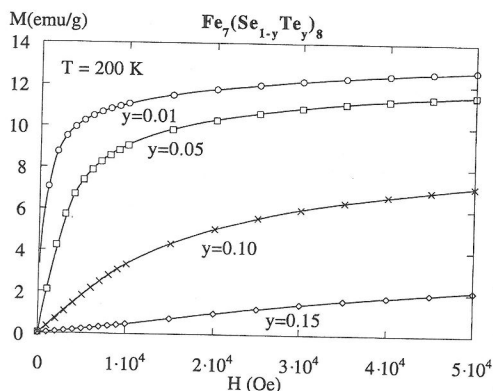


FIG. 5. Magnetization versus applied field H for four different samples of $\text{Fe}_7(\text{Se}_{1-y}\text{Te}_y)_8$ at 200 K.

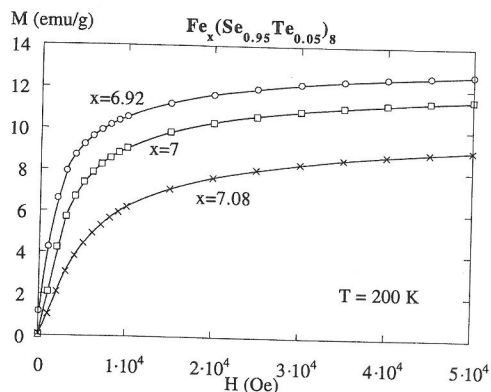


FIG. 7. Magnetization of $\text{Fe}_x(\text{Se}_{0.95}\text{Te}_{0.05})_8$ for three samples with $x = 6.92, 7$ and 7.08 versus applied field at $T = 200$ K.

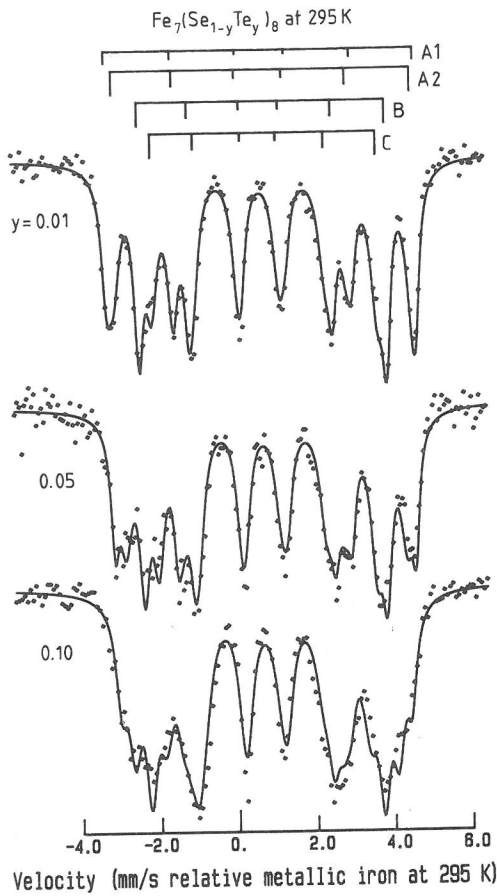


FIG. 8. Mössbauer spectra, recorded at room temperature of $\text{Fe}_7(\text{Se}_{1-y}\text{Te}_y)_8$ with $y = 0.01, 0.05$ and 0.10 . The spectra are fitted using four sextets A_1, A_2, A and C with intensities 1:2:2:2. The bar diagram above shows the peak-positions for $y = 0.01$.

$= -0.69$ T and $\Delta B_c = -3.75$ T (ERICSSON *et al.*, 1994). Assuming a random distribution of vacancies over the metal positions in Fe_7Se_8 should then result in a spectrum described by a broad sextet with a hyperfine field of ≈ 23 T and weak shoulders on the inner sides, coming from a broad sextet with a field of ≈ 19 T. None of our spectra can be fitted to such a model, and as a consequence we assume that vacancy-vacancy repulsion leads to short range order with A, B, and C like surroundings even for Te-rich compositions. The broad spectra obtained for $\text{Te} \geq 0.05$ can be understood as a result of the random Se-Te mixing in the anion shells surrounding the central iron atom. In the fittings the centroid shifts for A_1 and A_2 were constrained to equal values, and intensities of A_1, A_2, B and C patterns were fixed to 1:2:2:2. With increasing Te-

mixing, the half widths increase from 0.2 mm/s to 0.4 mm/s. $\text{CS}(A_1) = \text{CS}(A_2)$ are a few hundreds of a mm/s bigger than $\text{CS}(B) \approx \text{CS}(C)$, but the centroid shifts did not show any significant variation with composition, on average $\text{CS} = 0.715(10)$ mm/s in the whole interval. The quadrupole splittings (defined as $\text{DQ} = 0.5(v_6 - v_5 - v_2 + v_1)$, where v_1, \dots, v_6 are peak positions in the sextet with increasing velocity) are small but positive for all sites with no significant variation with composition: $\text{DQ}(A_1) = 0.05(5)$, $\text{DQ}(A_2) = 0.05(5)$, $\text{DQ}(B) = 0.05(5)$ and $\text{DQ}(C) = 0.13(3)$ mm/s.

The magnetic field is 28.7, 28.6, 27.4 and 25.9 tesla for the A_1, A_2, B and C sites in Fe_7Se_8 and decreases linearly to 21.7, 19.8, 17.4 and 14.9 tesla in $\text{Fe}_7(\text{Se}_{0.85}\text{Te}_{0.15})_8$ for the respective sites. Thus, the hyperfine field is the only Mössbauer parameter that shows a clear composition dependence in the studied interval.

Mössbauer spectra recorded at low temperatures. In $\text{Fe}_7\text{Se}_8 3c$, the room temperature quadrupole splittings are in the range 0–0.15 mm/s for the four sites: A_1, A_2, B and C . However, at temperatures around 100 K, the A_1 and A_2 patterns coincide and DQ is smaller (0, -0.3 and 0 mm/s for the A, B and C sites; (AMCOFF *et al.*, 1994; OK *et al.*, 1993). This can be understood as a result of the spin reorientation from the *ab*-plane to the *c*-axis with decreasing temperature. The same tendency is observed for the compositions studied here. Although the spectra are broadened due to the Se-Te mixing, DQ is close to or below zero at temperatures around 100 K, and positive, showing values some tenths of a mm/s higher, around 200 K. DQ is related to the electric field gradient (EFG) and the direction of the hyperfine field relative EFG, defined through the polar and azimuthal angles Θ and Φ :

$$\text{DQ} = \frac{V_{zz}eQ}{2} \left(\frac{3 \cos^2 \Theta - 1 + \eta \sin^2 \Theta \cos 2\Phi}{2} \right)$$

Here η is the asymmetry parameter and V_{zz} is the principal component of the EFG. In $\text{Fe}_7\text{Se}_8 3c$, on decreasing temperature, there is a decrease in DQ at 130 K of ≈ 0.3 mm/s (OK *et al.*, 1993). Thus, it is obvious that the substitution of Se by Te does not lead to a significant randomization of EFG directions relative to the magnetization direction. (The quadrupole splitting should not be sensitive to a spin rotation in such a case.)

Spectra recorded in the vicinity of liquid helium temperature are broadened compared to spectra at 100 K and above. To get reasonable fits we have used 8 sextets (with some constraints in order to

keep the number of free parameters low), three coming from A sites (thus having equal CS), two from B and C sites each, and a low field (≈ 12 tesla) sextet with 5% intensity at 128 K, increasing to 10% at 15 K. A component having an extraordinary low field has earlier been observed in Fe_7Se_8 (AMCOFF *et al.*, 1994). FATSEAS *et al.*, (1977) and BOUMFORD and MORRISH (1974) also noticed that Fe_7Se_8 spectra recorded at 4.2 K were more complex compared to the spectra recorded at 77 K. To get comparable parameter values, these eight sextets have been also used in fitting $\text{Fe}_7(\text{Se}_{0.90}\text{Te}_{0.10})_8$ at 200 K, 128 K and 15 K (see Fig. 9). The intensity-weighted averaged centroid shift, $\text{CS}_{\text{aver.}} = 0.86, 0.82$ and 0.77 mm/s at 15 K, 128 K and 200 K respectively, which gives a slope

of -7.8×10^{-4} mm/(s K) above 128 K. This is comparable with the high temperature slope of the second order dopplershift (SOD) of -7.3×10^{-4} mm/(s K) (COHEN, 1976). The Debye temperature of Fe_7Se_8 is low, 248(5) K (OK *et al.*, 1993), giving an increase in SOD of 0.04 mm/s from 128 K to 15 K, in full agreement with the experimental values above. $\text{DQ}_{\text{aver.}} = -0.08(2)$ mm/s below 128 K, and the hyperfine field $B_{\text{aver.}}$ increases from 22 T at 128 K to 23 T at 15 K. Fe_7Se_8 at 7 K and $\text{Fe}_7(\text{Se}_{0.85}\text{Te}_{0.15})_8$ at 15 K gave average hyperfine fields of 23.9 and 22.9 tesla, respectively. Thus, the clear difference in hyperfine fields with composition, as measured at room temperature, is probably a result of a decrease in magnetic ordering temperature T_N with increase in Te/Se substitution. (Our SQUID magnetometer cannot be used at temperatures above 300 K, so we have not yet studied how T_N varies with composition). Contrary to the observations above, OK *et al.* (1993) claimed that they had successfully fitted Mössbauer spectra of Fe_7Se_8 3c, recorded down to 12 K, using only three sextets.

DISCUSSION

The low field permeability

The magnitude of the magnetisation in an external field of 1 kOe decreases strongly with concentration of Te in $\text{Fe}_7(\text{Se}_{1-y}\text{Te}_y)_8$, at temperatures below T_{sr} more than 100 times and at temperatures above T_{sr} more than 50 times from $y = 0.01$ to $y = 0.15$, a change of order 25 times stronger than the corresponding decrease in $\text{Fe}_7(\text{Se}_{1-y}\text{S}_y)_8$. The magnetization increases also with concentration of vacancies in $\text{Fe}_x(\text{Se}_{1-y}\text{Te}_y)_8$. The fraction of vacant Fe-sites is given by $(8-x)/8$, *i. e.* 13.5%, 12.5% and 11.5% for $x = 6.92, 7$ and 7.08 , respectively. Using Fig. 7 (values for $\text{Fe}_x(\text{Se}_{0.95}\text{Te}_{0.05})_8$), and assuming that the magnetization values at an external field of 5 tesla are proportional to the saturation value, one gets the following ratios between saturation magnetization and concentration of vacancies: 12.8 (emu/g)/13.5% = 0.95, 11.5 (emu/g)/12.5% = 0.92 and 9 (emu/g)/11.5% = 0.78. The nearly equal value of the ratio for the two more vacancy-rich samples can be interpreted to reflect a similar degree of vacancy ordering in alternate *ab* layers in those samples. The significantly lower ratio between saturation magnetization and number of vacancies for the 11.5% sample may be understood as a result of a less ideal 3c structure in this sample. In this respect it is interesting to note that the homogeneity range for the 3c structure can be expected to move to the vacancy-rich side of a nominal $\text{Fe}_7(\text{Se}, \text{Te})_8$

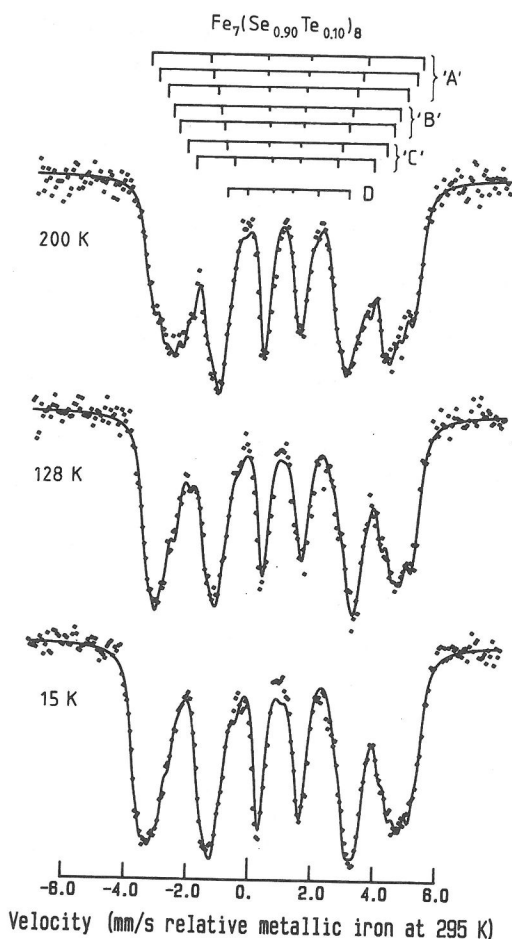


FIG. 9. Mössbauer spectra, recorded at 200 K, 128 K and 15 K of $\text{Fe}_7(\text{Se}_{0.90}\text{Te}_{0.10})_8$. All spectra are fitted using 8 sextets, assigned to 'A', 'B', 'C' and D sites. For further details, see text.

composition as the concentration of Te increases (IPSER *et al.*, 1974). The low ratio between saturation magnetization and concentration of vacancies for $x = 7.08$ is also in agreement with results for pure Fe selenides, showing a rapid decrease in this ratio with decrease in number of vacancies (AMCOFF *et al.*, 1994).

A simple model

Our XRD, SQUID and MS results can all be described in the following schematic way. In $\text{Fe}_7\text{Se}_8 3c$, the vacancies are confined to every second metal *ab*-layer. The antiferromagnetic coupling between the layers and the ferromagnetic coupling within a layer give ferrimagnetism, and the net magnetization of a domain is given by the difference in magnetization of vacancy-free layers and vacancy layers (see Fig. 10). When S, and especially Te, is substituted into the system, the size of the ordered regions decreases and phase and antiphase regions start to coexist within a magnetic domain. The randomly distributed Te (or S) anions hinder the diffusion of vacancies. The macroscopic magnetization will now depend on the difference in "phase volume" (PV) and "anti phase volume" (APV) within a magnetic domain. With increasing S and Te substitutions, the number of phase and antiphase domains within a magnetic domain increases rapidly (Fig. 10). This leads to a comparably low value of the permeability. The results (see *e.g.* Fig. 4) also indicate a significant increase in anisotropy when the spins are aligned along the *c* axis as compared to in-plane alignment. The smaller individual PVs and APVs result in a lack of supercell reflections in XRD and also give a magnetically harder material, as the magnetization of a magnetic domain decreases significantly with S/Se or Te/Se substitution. Still, there is local ordering of vacancies around an individual iron atom, leading to A, B and C like surroundings as shown by the Mössbauer spectra above. The broadening in MS for Te-rich samples could both be due to the Se/Te mixing and to the increasing numbers of phase-antiphase boundaries.

The spin reorientation

The spin reorientation temperature T_{sr} increases with decreasing number of vacancies (Fig. 6) and with increasing Te/Se substitution (Fig. 4). The covariation of *a/c* and T_{sr} with anion substitution (Fig. 11), as well as with concentration of vacancies, indicates a geometrical factor for the dependence

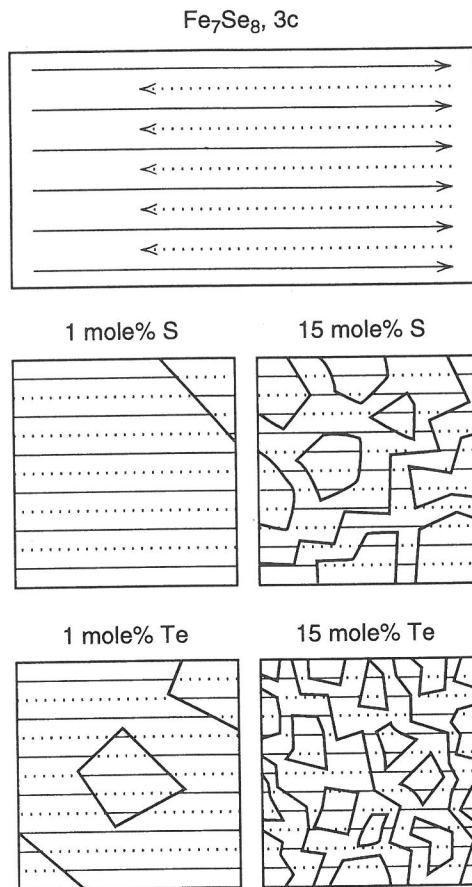


FIG. 10. A schematic model for magnetization of $\text{Fe}_7(\text{Se}_{1-x}\text{X}_x)_8$, with $\text{X} = \text{S}$ or Te above the spin reorientation temperature. The rectangles denote a magnetic domain with a ferromagnetic coupling within an *ab* layer passing the phase-antiphase border. The situation in ideal $3c$ is visualized at top. Due to 25 % vacancies in every second cation layer (dotted lines) there is a ferrimagnetic moment and a net macroscopic magnetisation. The number of phase-antiphase borderlines within the magnetic domain will increase with concentration of S and especially with Te, giving a reduced macroscopic magnetisation (middle and bottom pictures).

of T_{sr} with composition. Low temperature favors spins parallel with the *c*-axis and high temperatures spins in the *ab*-plane. Apparently, short distances within the *ab*-plane or in the *c* direction favor spin orientation in the *ab*-plane or parallel to the *c*-axis, respectively.

A spin reorientation also appears in related systems. T_{sr} is suppressed to ≈ 0 K for $\text{Fe}_7(\text{Se}_{0.4}\text{S}_{0.6})_8$, thus there is no spin reorientation in ordinary pyrrhotite. However, there is a similar spin transition in FeS at 445 K, with a decrease of 40 K for each

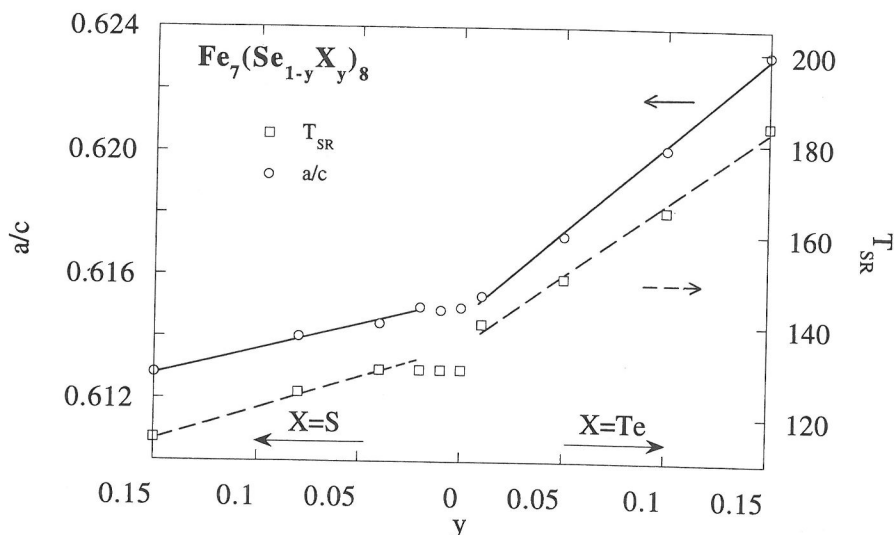


Fig. 11. Ratio of the lattice parameters a/c (left axis) and spin reorientation temperature, T_{sr} (right axis), plotted vs concentration of anion substitution y for $\text{Fe}_7(\text{Se}_{1-y}\text{X}_y)_8$. Data are shown for $X = \text{S}$, (left part of the x axis) and $X = \text{Te}$, (right part of the x axis).

% of metal vacancies on the sulfur-rich side (HORWOOD *et al.*, 1976). Thus, increases in concentration of vacancies decrease T_{sr} in FeS as well as in the system $\text{Fe}_x(\text{Se}_{1-y}\text{Te}_y)_8$. In $(\text{Fe}_{1-y}\text{Co}_y)_7\text{Se}_8$ the spin transition temperature increases with y , in $(\text{Fe}_{0.92}\text{V}_{0.08})_7\text{Se}_8$ 4c, the spin reorientations occurs abruptly at 123 K, while there is a continuous change below 220 K in Fe_7Se_8 4c (SATO *et al.*, 1985 and OK *et al.*, 1994). XRD data at low temperatures might improve our understanding of the spin rotation mechanism, and both cation as well as anion substitutions may give hints to explain the spin reorientation in ordinary pyrrhotites as well.

Mineralogical considerations

The present results show that substitution of anions with identical charges in Fe_7Se_8 affects ordering processes in cation positions and that the magnitude of this effect, among other factors, depends on chemical differences between the anions. Indirectly, it can be inferred that substitution of ions in *any* variable position in a crystal structure affects other variable positions in the structure in ways that are not always obvious. The idea presented here of "induced disorder" may be of importance, especially in relation to order-disorder geothermometry and order-disorder geospeedometry, as natural minerals are invariably "contaminated" by foreign atoms which may act as "nuclei of disorder".

Acknowledgements—This investigation was supported by the Swedish Natural Science Research Council.

REFERENCES

- AMCOFF Ö., ERICSSON T. and GISMELSEED A. (1994) An X-ray, Mössbauer and magnetization investigation of hexagonal FeSe. *Zeits. Krist.* **209**, 197–205.
- BARKER W. W. and PARKS, T. C. (1986) The thermodynamic properties of pyrrhotite and pyrite. A re-evaluation. *Geochim. Cosmochim. Acta* **50**, 2185–2194.
- BERTAUT E. F. (1953) Contribution à l'étude des structures lacunaires: La pyrrhotine. *Acta Crystallo.* **6**, 557–561.
- BOUMFORD C. and MORRISH A. H. (1974) Magnetic properties of the iron selenide Fe_7Se_8 . *Phys. Stat. Sol. (a)* **22**, 435–444.
- COHEN R. L. (1976) *Application of Mössbauer spectroscopy, volume I*. Academic Press, New York San Francisco London.
- ERICSSON T., AMCOFF Ö. and NORDBLAD P. (1994) Vacancy ordering in Fe_7Se_8 - Fe_7S_8 solid solutions studied by Mössbauer, X-ray and magnetization techniques. *Hyper. Interact.* **90**, 515–520.
- FATSEAS G. A., DORMANN J. L., DRUILHE R., BROSSARD L. and GIBART P. (1977) Test of the "3c" and "4c" Fe_7Se_8 Okazaki's superstructures by Mössbauer effect. *Physica* **86-88B**, 887–888.
- HORWOOD J. L., TOWNSEND M. G. and WEBSTER A. H. (1976) Magnetic susceptibility of single crystal Fe_{1-x}S . *J. Solid State Chem.* **17**, 35–42.
- IGAKI K., SATO M. and SHINOHARA T. (1981) Mössbauer study on the iron vacancy distribution in iron sulfide Fe_{1-x}S ($0.083 \leq x \leq 0.125$). *Trans. JIM* **22(9)**, 627–632.
- IGAKI K., SATO M. and SHINOHARA T. (1982) Mössbauer study on the distribution of iron vacancies in iron sulfide Fe_{1-x}S . *Trans. JIM* **23(5)**, 221–228.

- IPSER H., KOMAREK K. L. and MIKLER H. (1974) Transition metal—chalcogen systems, V.: The iron-tellurium phase diagram. *Mh. Chem.* **105**, 1322–1334.
- JERNBERG P. and SUNDQVIST T. (1983) A versatile Mössbauer analysis program. *Inst. Phys. Reports* 1090, University of Uppsala.
- KISSIN S. A. and SCOTT S. D. (1982) Phase relations involving pyrrhotite below 350°C. *Econ. Geol.* **77**, 1739–1754.
- KRUSE O. (1990) Mössbauer and X-ray study of the effects of vacancy concentration in synthetic hexagonal pyrrhotites. *Amer. Mineral.* **75**, 755–763.
- KULLERUD G. (1986) Monoclinic pyrrhotite. *Bull. Geol. Soc. of Finland* **58**, 293–305.
- LEVINSON L. M. and TREVES D. (1968) Mössbauer study of the magnetic structure of Fe₇Se₈. *J. Phys. Chem. Solids* **29**, 2227–2231.
- OK H. N., BAEK K. S. and KIM E. C. (1993) Mössbauer study of “3c” superstructure of the ferrimagnetic Fe₇Se₈. *Solid State Commun.* **87**, 1169–1172.
- OK H. N., BAEK K. S. and PARK E. B. (1994) Effects of vanadium impurities on the spin-rotation transition of iron selenide “4c” Fe₇Se₈. *Solid State Commun.* **92**, 459–461.
- PUTNIS A. and MCCONELL J. D. (1980) *Principles of Mineral Behaviour*. Blackwell Scientific Publications.
- SATO M., KAMIMURA T. and IWATA T. (1985) Magnetic properties of (Fe_{1-x}Co_x)₇Se₈. *J. Appl. Phys.* **57**(1), 3244–3246.
- SCHUSTER W., MIKLER H. and KOMAREK K. L. (1979) Transition metal-chalcogen systems. VII.: The iron-selenium phase diagram. *Mh. Chem.* **110**, 1153–1170.
- THIEL R. C. (1969) A Mössbauer study in the troilite-pyrrhotite system. *Ph. D.-thesis*, Rijksuniversiteit te Groningen, Netherlands.
- VAUGHAN D. J. and CRAIG J. R. (1978) *Mineral chemistry of metal sulfides*. Cambridge University Press.